Physica B 152 (1988) 105–112
North-Holland, Amsterdam

$T_c(H)$ FOR QUASICRYSTALLINE MICRONETWORKS: ANALYTICAL AND NUMERICAL RESULTS

Franco NORI and Qian NIU
Institute for Theoretical Physics, University of California, Santa Barbara, CA 93106, USA

We report on some analytical and numerical results, on the study of flux quantization in aperiodic superconducting arrays. In particular, the superconducting–normal phase boundary, $T_c(H)$, is calculated and the origin of its overall and fine structure is analyzed as a function of the network size. We also propose a new way of analytically analyzing the overall and the fine structure of $T_c(H)$ in terms of short- and long-range correlations among tiles. Some of the results obtained are compared with experimental measurements done by, in alphabetical order, the groups of Chaikin, Pannetier, and Van Harlingen.

1. Introduction

Micronetworks made of thin superconducting wires [1], proximity-effect junctions [2], and tunnel junctions [3], exhibit interesting forms of phase diagrams when they are immersed in an external magnetic field. The diamagnetic properties of such micronetworks are very sensitive to the geometry of the multiply-connected structure. Fractal [4], disordered and quasicrystalline [5–8] geometries have recently been investigated by different groups.

Here, we study the frustration induced in 2D quasicrystalline networks by an applied magnetic field, and its effect on their superconducting diamagnetic properties. In particular, we calculate the superconducting–normal phase boundary, $T_c(H)$, for several of the 2D geometries which have been studied experimentally [5–7, 9]. The agreement between our curves and the experimental data [5–7, 9] obtained so far is very good. In particular, we study step-by-step in a progressive way, the effect of adding more and more tiles to the basic cells of the samples.This approach allows us to gain insight about the origin of the overall and fine structure present in $T_c(H)$. Furthermore, we propose a new analytical and systematic way of analyzing the structure of the phase boundaries in terms of correlations among tiles.

The ratio of the elementary plaquette areas is equal to an irrational number for all the lattices considered here. This geometric constraint implies that the magnetic flux cannot satisfy quantization in all the plaquettes simultaneously (see also ref. [9]). Thus, a continuous variation of the applied magnetic field allows the unique possibility for a fine tuning of the geometry-induced frustration. We have considered the linearized Ginzburg–Landau equations [11] (for the superconducting networks) and the linearized mean-field approximation to the frustrated XY Hamiltonian [12] (for the Josephson-junction array). Both of them can be formally written [11, 12] as a tight-binding Schrödinger equation:

$$\sum_{\beta} J_{\alpha\beta}\, e^{iA_{\alpha\beta}}\psi_{\beta} = \epsilon\psi_{\alpha} ,$$

where $A_{\alpha\beta} = (2\pi/\Phi_0)\int_{\alpha}^{\beta} \boldsymbol{A}\cdot d\boldsymbol{l}$, and $\Phi_0 = ch/2e$. The highest eigenvalue is proportional to $T_c(H)$.

For the sake of brevity, we will concentrate here on three types of geometries (1) periodic along one direction and quasicrystalline in the other direction (strip geometry); (2) Penrose lattice (see fig. 1(a)); and (3) eightfold Penrose lattice (see fig. 1(b)) [10]. For these two networks, the ratio of basic frequencies in the diffraction pattern is equal to the golden mean,

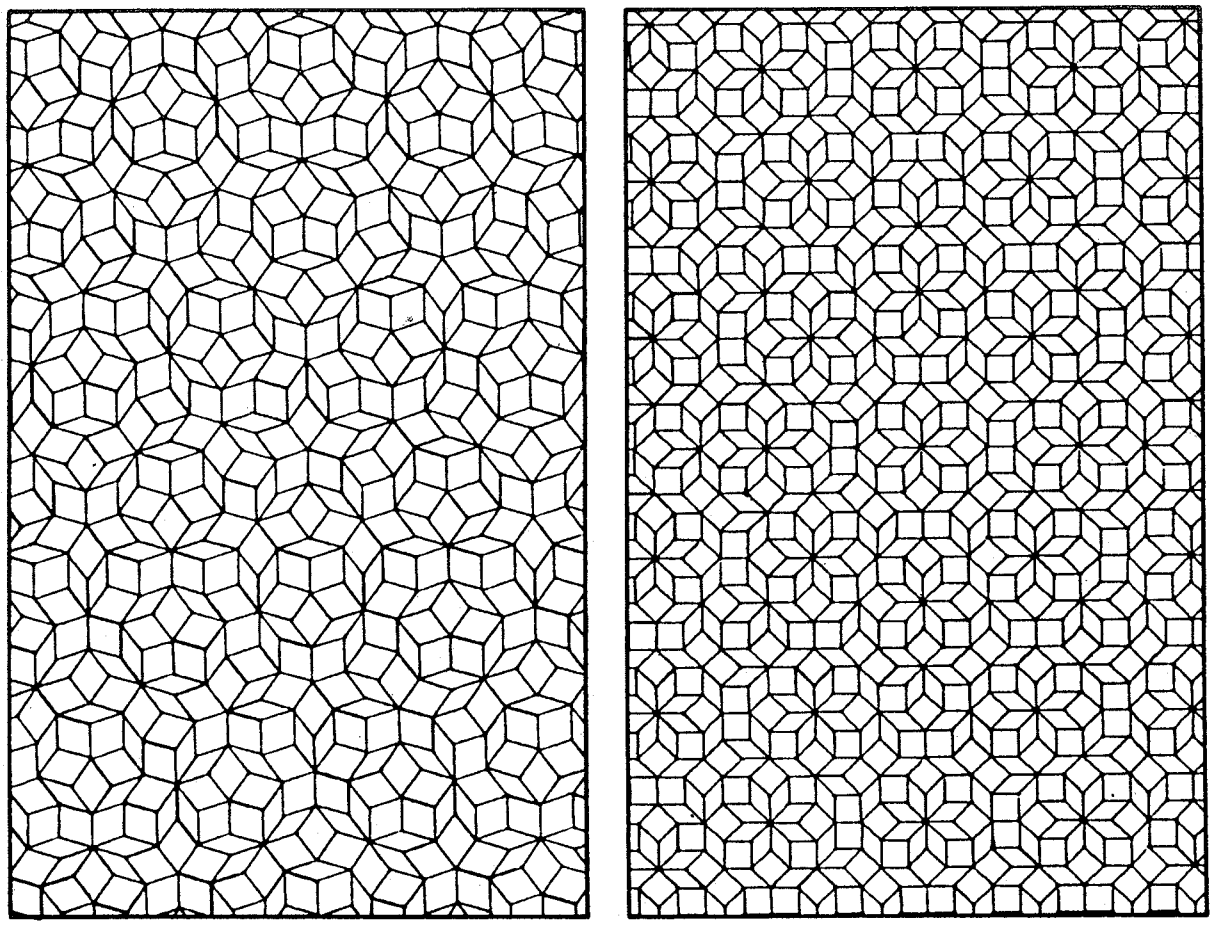

Fig. 1. (a) Portion of a Penrose pattern. (b) Portion of an eightfold Penrose pattern.

$\tau \equiv (\sqrt{5}+1)/2 = 2\cos(\pi/5)$, and the two types of elementary plaquettes have a ratio of areas (large to small) and a population ratio (number of large to number of small tiles) both equal to τ. We have also studied the 1D analog of the 2D eightfold symmetric quasicrystalline lattice [8]. The silver mean, $\zeta = \sqrt{2}+1 = \cot(\pi/8)$, characterizes the quasiperiodicity of these two networks. The ratio of areas and the population ratio, for these two lattices, are equal to $\sqrt{2}$ and $1/\sqrt{2}$, respectively. De Bruijn [10] first gave a global prescription to generate 2D Penrose patterns. We constructed our fivefold (eightfold) Penrose lattices by projecting a 5 (8) dimensional hypercubic grid into a 2D subspace. The centers of the hypercubes which intersect a particular hypersurface are projected into it.

2. Fibonacci strips

In order to obtain $T_c(H)$ for the 2D Fibonacci lattice, it is convenient to use the Landau gauge $\boldsymbol{A} = Bx\hat{y}$, in which an eigenfunction of our tight-binding equation takes the product form $\eta_{nm} = \psi_n e^{ikm}$, where ψ_n satisfies the 1D equation:

$$\frac{2k_B T}{J}\psi_n = \psi_{n+1} + \psi_{n-1} + 2\cos(2\pi f x_n - k)\psi_n ,$$

with $f = \Phi_s/\Phi_0$ (or $f\tau$) being the reduced magnetic flux, i.e. the magnetic flux through a small (large) cell divided by the flux quantum. For a fixed value of k, we numerically solve the above equation for the largest eigenvalue, which is then maximized by varying k in the range $(0, \pi)$ to find the transition temperature.

The transition from a *periodic* phase boundary $T_c(H)$ to the richly structured one associated with an underlying QC geometry can be followed in fig. 2. The associated lattices have a strip-type geometry. The ratio of the elementary plaquette areas is equal to the golden mean. The minima and maxima of the $T_c(H)$ curve, for the periodic ladder geometry with only one type of cell (fig. 2(a)), are quadratic. However, the local maxima and minima for the quasicrystalline strip systems (fig. 2(b–e)) tend, in general, to be more peaked (cusp-like). This suggests that one-cell effects are responsible for the quadratic (parabolic) extrema, meanwhile the cusp-like behavior is due to the collective effect of many cells. Fig. 2(b) shows the $T_c(H)$ curve for a strip with two types of elementary plaquettes. From it, we note that only the main features of the 2D Fibonacci and Penrose lattices phase boundaries are essentially determined by the irrationality of the ratio of the elementary plaquette areas. If we increase the number of tiles, we obtain more and more fine structure. Below, we will come back to this point through analytical means.

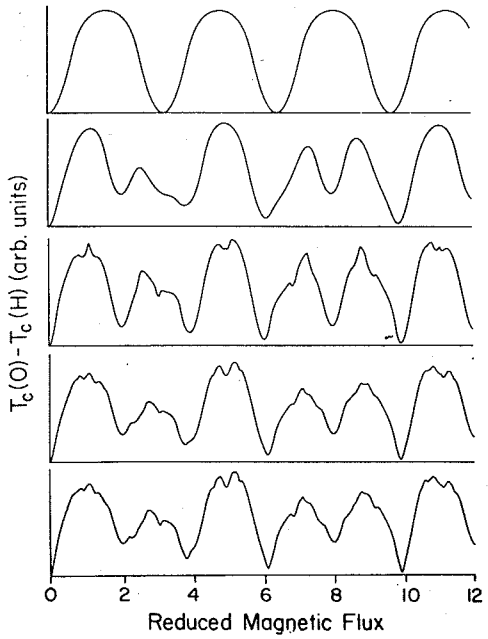

Fig. 2. Phase boundary for lattices with strip-type geometry. The number of quasicrystalline spaced vertical lines is equal to successive Fibonacci numbers: (a) 2 vertical lines (ladder network); (b) 3; (c) 5; (d) 8; and (e) 13.

3. Superconducting Penrose arrays

The use of a periodic direction greatly simplifies the calculations. However, neither the Penrose nor the eightfold Penrose lattices have periodic directions. Obtaining $T_c(H)$ for these lattices is more difficult since these two systems *cannot* be simplified by using translational invariance and, therefore, the problem needs to be tackled directly. We have numerically solved the linearized Ginzburg–Landau equations for a Penrose lattice with 301 nodes (dotted line in fig. 3) and for an eightfold Penrose lattice with 329 nodes (dotted line in fig. 4). This is equivalent to solving the linearized mean-field equations for the XY Hamiltonian, or solving the electronic tight-binding problem; and then plotting the edge state versus magnetic field. Our choice of gauge was

$$A_{\alpha\beta} = \frac{2\pi}{\Phi_0} B(y_\beta - y_\alpha)(x_\alpha + x_\beta)/2 ,$$

where x_α and y_α are the coordinates of the αth node. The continuous line in fig. 3 is experimental data obtained by Springer and Van Harlingen [6] for an array of 14 000 weakly-coupled superconducting islands fabricated using direct-write

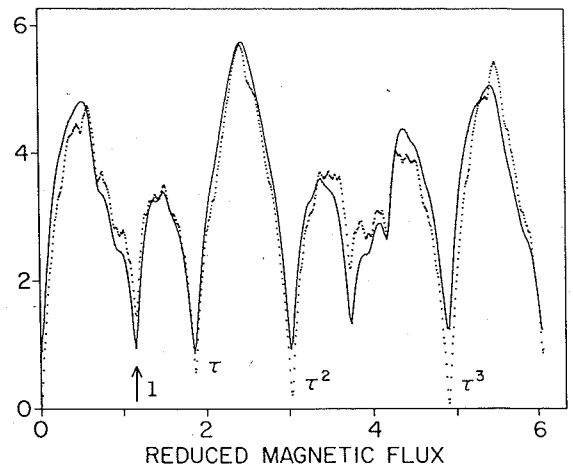

Fig. 3. Superconducting–normal phase boundary for the Penrose pattern. The solid line is experimental data for a Josephson-junction array (ref. [4]), and the points are our theoretically obtained values for a lattice with 301 nodes. The vertical axis represents voltage (10 nV) for the experimental data, and $T_c(0) - T_c(H)$ (arb. units) for the theory.

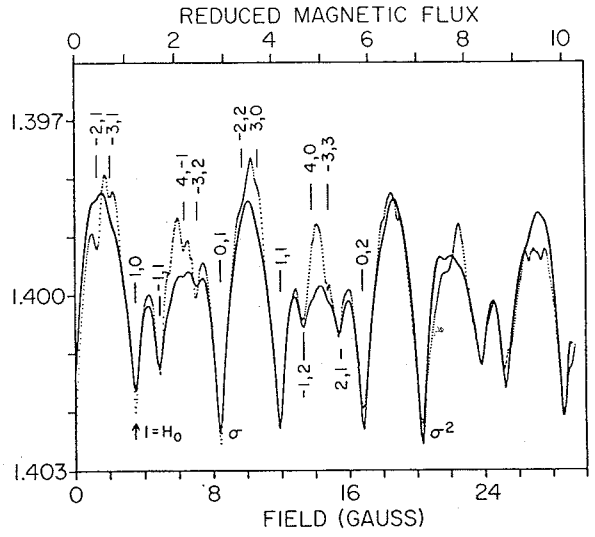

Fig. 4. Phase boundary, $T_c(0) - T_c(H)$, for the eightfold Penrose pattern. The solid line is experimental data (K) for an aluminum wire micronetwork (ref. [3]), and the points are our theoretically obtained values (arb. units) for a lattice with 329 nodes.

electron-beam lithography. They measured the voltage across the sample (which follows the behavior of $-T_c(H)$) versus applied transverse magnetic field. In fig. 3 we have plotted our theoretical curve and their data, obtained for a voltage bias of around 40 nV. The agreement between them is very good. Also, detailed comparison with the data of Pannetier's group [7] has given a very good agreement even for the fine structure found at small fields. For the 2D Fibonacci geometry, and also for the Penrose array case, an average flux of one flux quantum per elementary tile corresponds [5] to an applied magnetic field of $H_0 = \Phi_0(1+\tau^{-2})^{-1}/a_s$, where a_s = area of a small tile. An arrow in fig. 3 indicates the small dip associated with this field ($H/H_0 = 1$). Also, the average applied field in order to have $N_l(N_s)$ flux quanta in every large (small) tile is:

$$H = \Phi_0(N_s + \tau N_l)(1+\tau^2)^{-1}/a_s\,.$$

Therefore, the arrangements of the flux quanta [5] on the array are $(N_s, N_l) = (1,1)$, $(1,2)$, $(2,3)$, and $(3,5)$ for the indicated values of the magnetic field, i.e. $H/H_0 = 1$, τ, τ^2 and τ^3, respectively.

Let us now consider the eightfold symmetric network shown in fig. 1(b). The continuous line in fig. 4 is experimental data obtained by Behrooz et al. [5]. The arrow indicates the magnetic field corresponding to one flux quantum in each elementary tile $H_0 = \Phi_0(1+\sqrt{2})/(2a_s)$. The fields $H = \Phi_0(N_l + \sqrt{2}N_s)/2a_s$ have been indicated by $(N_l, N_s) = (1,1)$, $(3,2)$, and $(7,5)$ for $H/H_0 = 1$, ζ, and ζ^2, respectively. The fields corresponding to $n + m\zeta$ for $|n|$, $|m| < 4$ (see fig. 4) account for most of the theoretical and experimental fine structure.

4. Analytical approach and conclusions

So far, all our theoretical data were obtained numerically. However, we have also employed a novel way to obtain and explain the basic features of $T_c(H)$. This approach, based on the Lanczos method [13], is designed to approximate the largest eigenvalue (to be denoted as $E_0(H)$) for our eigenvalue equations. As we will see, this method is not only simple, but also makes explicit the physical origin of the peaks and valleys of various sizes in $T_c(H)$. First, we choose a state ψ_1 which is uniform on the lattice. Afterwards, a second state ψ_2 is obtained as $Q_1(\hat{H}\psi_1)$, where Q_1 projects off the space spanned by ψ_1. If we replace the full Hamiltonian, $\hat{H}$, by its restriction, $\hat{H}_2$, on the linear manifold spanned by $\{\psi_1, \psi_2\}$, then the larger eigenvalue of $\hat{H}_2$ (which approximates $E_0(H)$) gives a fairly good result in locating the relative heights of the main peaks and dips of the $T_c(H)$ curve. If we go one step further, i.e. to define $\psi_3 = Q_2Q_1(\hat{H}\psi_2)$ and replace $\hat{H}$ by its restriction, $\hat{H}_3$, on the linear manifold spanned by $\{\psi_1, \psi_2, \psi_3\}$, then the largest eigenvalue of $\hat{H}_3$ gives a much better approximation to $E_0(H)$ and most of the fine structure is reproduced, in addition to the main peaks and dips. In general, higher order truncations of the Hamiltonian produce better results, revealing finer structures. In order to make the following discussion more specific, we will now

consider a strip-type geometry as an example. A uniform state ψ_1 generates the following equations:

$$\hat{H}\psi_1 = 2\psi_1 + 2\psi_2 , \tag{1}$$

$$\hat{H}\psi_2 = \psi_1 + C\psi_2 + \psi_3 , \tag{2}$$

$$\hat{H}\psi_3 = D\psi_2 + F\psi_3 + \psi_4, \ldots ; \tag{3}$$

where

$$C = 2\langle \cos 2\pi f L_n \rangle , \tag{4}$$

$$D = 3 - C^2 + 2\langle \cos 2\pi f(L_n + L_{n+1}) \rangle , \tag{5}$$

$$\begin{aligned} F = (&C^3 - C + 2\langle \cos 4\pi f(L_n + L_{n+1}) \rangle \\ &- 4C\langle \cos 2\pi f(L_n + L_{n+1}) \rangle \\ &+ 2\langle \cos 2\pi f(L_n + L_{n+1} + L_{n+2}) \rangle)/D . \end{aligned} \tag{6}$$

We have used the Landau gauge as before, and the angular brackets denote averages along the horizontal direction (L_n are the lattice spacings). For instance, for the particular case of the Fibonacci network:

$$\langle \cos 2\pi f(L_n + L_{n+1}) \rangle = \frac{2}{\tau^2} \cos 2\pi f(L + S) + \frac{1}{\tau^3} \cos 4\pi f L , \tag{7}$$

and

$$\begin{aligned} &\langle \cos 2\pi f(L_n + L_{n+1} + L_{n+2}) \rangle \\ &= \left(\frac{1}{\tau} + \frac{1}{\tau_3}\right) \cos 2\pi f(2L + S) \\ &\quad + \frac{1}{\tau^4} \cos 4\pi f(L + 2S) . \end{aligned} \tag{8}$$

The largest eigenvalues, which approximate $T_c(H)$, for the second-, third-, and fourth-order truncation of the Hamiltonian have been plotted in fig. 5. The second-order truncation is already very good, reproducing the overall structure. As we proceed to higher orders, finer structure begins to emerge and develop. In order to see why this is the case, note that in the second-order truncation only the single-cell statistics (through C) comes in, while in the third-order trunction, correlations between *nearest* and *next* nearest neighboring cells are involved (through D and F), and the fourth-order truncation depends on even *longer* range correlations. We have therefore *proved* that the overall structure in $T_c(H)$ is a result of single-cell statistics. The above relations also prove, by considering successive higher order truncations, that longer range correlations among cells are responsible for the finer structure. This result is consistent with experimental [6] results obtained from the evolution of fine structure in Penrose lattices as a function of voltage bias. A complete and detailed exposition of this approach will be presented in full length elsewhere, including also the computed $T_c(H)$ curves for all the geometries studied experimentally [5]. Furthermore, a detailed analysis of the relationship between the full tight-binding electronic spectra (see figs. 6 and 7 for a crystalline and quasicrystalline example) and the $T_c(H)$ curve will also be presented elsewhere.

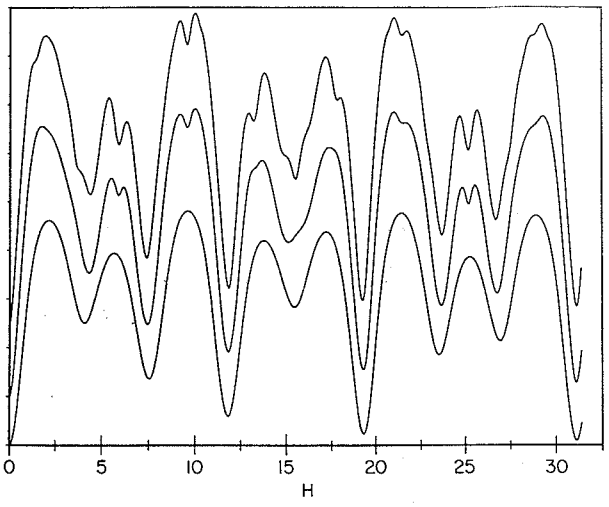

Fig. 5. Largest eigenvalues, obtained by using the Lanczos method, of the operators $\hat{H}_2$ (bottom), $\hat{H}_3$, and $\hat{H}_4$ (top) versus H for the 2D Fibonacci lattice. The vertical axis represents $T_c(0) - T_c(H)$ in arbitrary units. The curves have been shifted vertically in order to visualize them better.

The principal results we have obtained are (1) numerical calculations, which did not require a single adjustable parameter, of the supercon-

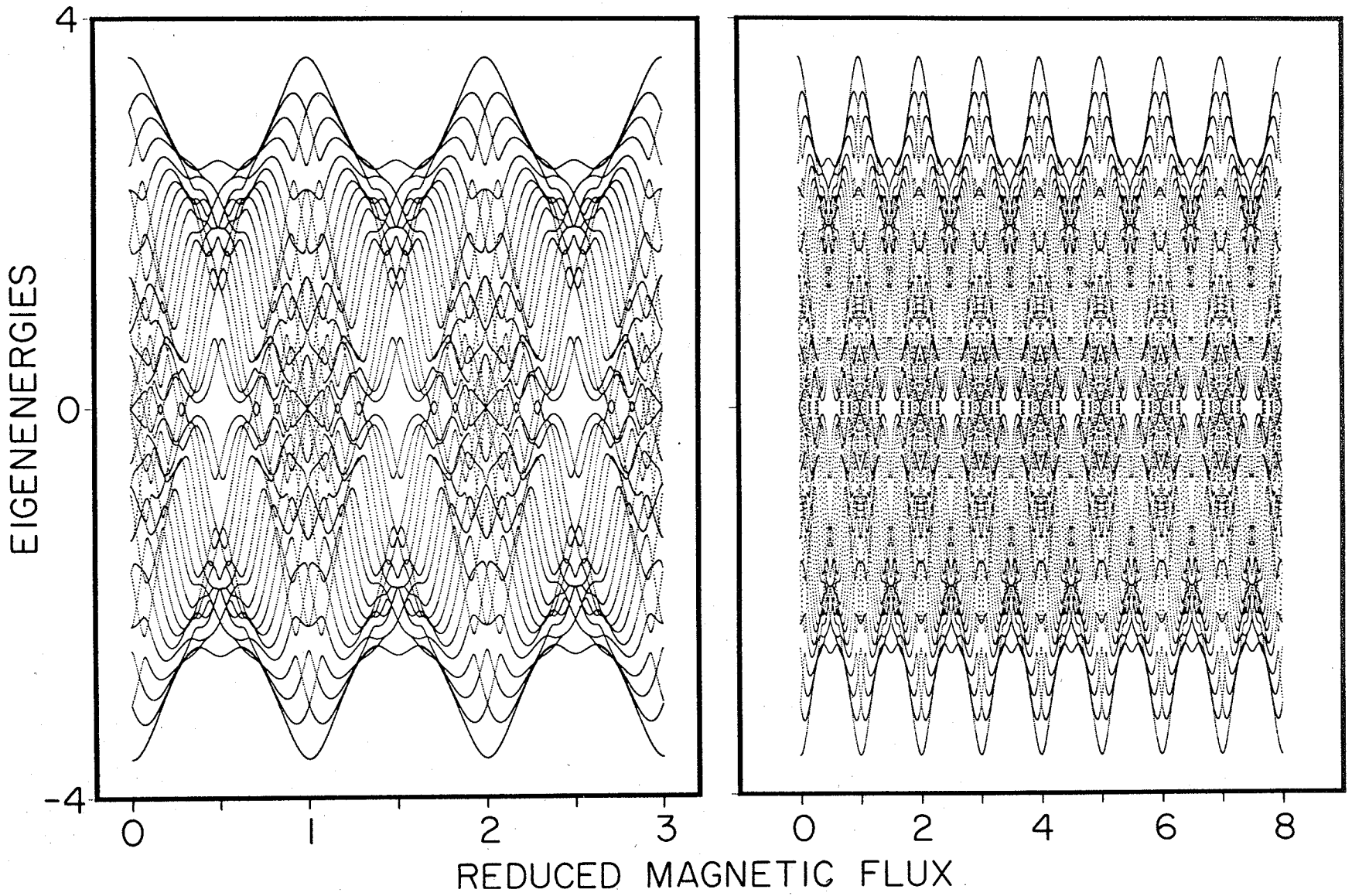

Fig. 6. Energy spectra versus applied magnetic field for a tight-binding electron hopping on a 6×6 square lattice. The horizontal axis represents the number of flux quanta per elemental square cell.

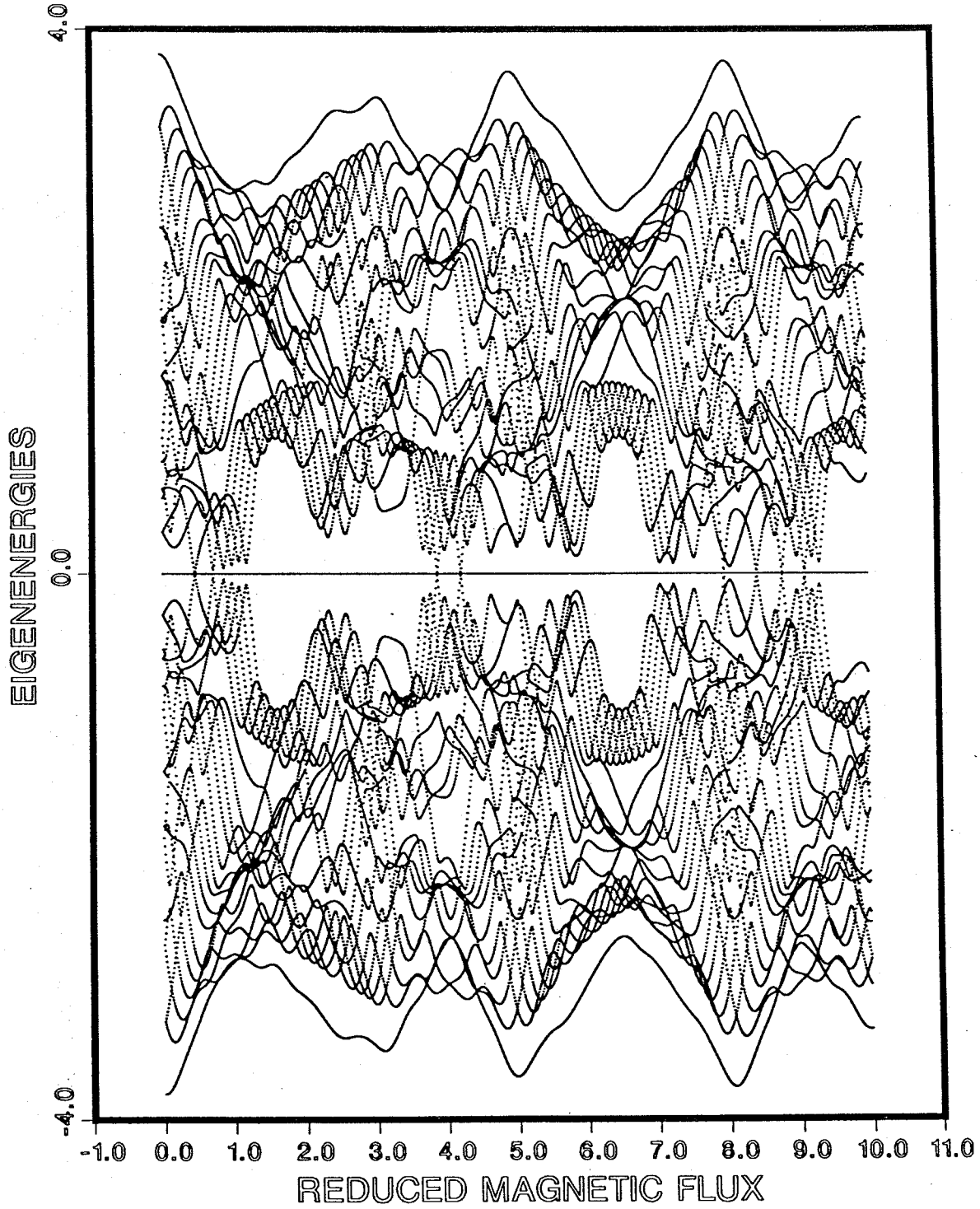

Fig. 7. Energy spectra versus applied magnetic field for a tight-binding electron hopping on a Penrose lattice with 46 sites.

ducting–normal phase boundary for the quasicrystalline systems fabricated by several experimental groups; (2) a very good agreement between our theoretical results and the experimental ones; and (3) a proposed new analytic and systematic way of analyzing $T_c(H)$ which for the first time explicitly shows, in a detailed and specific manner, the way short-range correlations among tiles affect the main peaks, and the way longer range correlations generate finer structure. Finally, some concluding comments are necessary. In our analysis, we have neglected superconducting fluctuations. Nevertheless, we do not expect them to be very important here because it is known that periodic superconducting arrays [1–3] in a transverse magnetic field display mean-field-like behavior. On the other hand, the size of the lattices we have studied is either one or two orders of magnitude smaller than the ones studied experimentally. We believe that this factor, together with the imperfections of the fabricated structures (e.g. the non-uniform width of the wires), account for most of the discrepancies between theory and experiment. Also, the finite width of the strands and the finite measurement current through the sample may smooth out some of the unobserved fine structure.

Acknowledgements

We are very grateful to P. Chaikin, B. Pannetier, P. Santhanam, and D. Van Harlingen for sharing with us their published and unpublished data and for useful discussions. Also, we acknowledge a collaboration with E. Fradkin and S.-J. Chang. This research was supported in part by the National Science Foundation under grant PHY82-17853, supplemented by funds from the National Aeronautics and Space Administration, and by DOE through grant DE84-ER-45108.

References

[1] B. Pannetier, J. Chaussy, R. Rammal and J. Villegier, Phys. Rev. Lett. 53 (1984) 1845; B. Pannetier, J. Chaussy and R. Rammal, J. Phys. (Paris) 44 (1983) L853.

[2] D.J. Resnick, J.C. Garland, J.T. Boyd, S. Shoemaker and R.S. Newrock, Phys. Rev. Lett. 47 (1982) 1542; C.J. Lobb, D.W. Abraham, M. Tinkham and T.M. Klapwijk, Phys. Rev. B 26 (1982) 5268; C.J. Lobb, D.W. Abraham and M. Tinkham, Phys. Rev. B 27 (1983) 27; D. Kimhi, F. Leyraz and D. Ariosa, Phys. Rev. B 29 (1984) 1487; R.K. Brown and J.C. Garland, Phys. Rev. B 33 (1986) 7827; Ch. Leeman, Ph. Lerch, G.-A. Racine, and P. Martinoli, Phys. Rev. Lett. 56 (1986) 1291.

[3] R.F. Voss and R.A. Webb, Phys. Rev. B 25 (1982) 3446; R.A. Webb, R.F. Voss, G. Grinstein and P.M. Horn, Phys. Rev. Lett. 51 (1983) 690; B.J. van Wees, H.S.J. van der Zant and J.E. Mooij, Phys. Rev. B 35 (1987) 7291.

[4] J.M. Gordon, A.M. Goldman, J. Maps, D. Costello, R. Tiberio and B. Whitehead, Phys. Rev. Lett. 56 (1986) 2280; J.M. Gordon and A.M. Goldman, Phys. Rev. B 35 (1987) 4909.

[5] A. Behrooz, M. Burns, H. Deckman, D. Levine, B. Whitehead and P.M. Chaikin, Phys. Rev. Lett. 57 (1986) 368; Phys. Rev. B 35 (1987) 8396.

[6] K. Springer and D. Van Harlingen, Phys. Rev. B 36 (1987) 7273.

[7] Y.Y. Wang, R. Steinmann, J. Chaussy, R. Rammal and B. Pannetier, Proc. LT 18, Kyoto (in press).

[8] F. Nori, Q. Niu, E. Fradkin and S.J. Chang 36 (1987) 8338; J. Chung, M.Y. Choi and D. Stroud, unpublished; Kalugin, Kitaev and Levitov, unpublished.

[9] P. Santhanam, C.C. Chi and W.W. Molzen, Phys. Rev. B 37 (1988) 2360; F. Nori and Q. Niu, Phys. Rev. B 37 (1988) 2364.

[10] N. de Bruijn, Ned. Akad. Weten. Proc. Ser. A 43 (1981) 27, 53; D. Levine and P.J. Steinhardt, Phys. Rev. B 34 (1986) 596, 617; for further studies of the 1D analog case see, for instance, F. Nori and J.P. Rodriguez, Phys. Rev. B 34 (1986) 2207; Q. Niu and F. Nori, Phys. Rev. Lett. 57 (1986) 2057.

[11] S. Alexander, Phys. Rev. B 27 (1983) 1541; R. Rammal et al., Phys. Rev. B 27 (1983) 2820; J. Simonin et al., Phys. Rev. Lett. 56 (1986) 2649.

[12] W.Y. Shih and D. Stroud, Phys. Rev. B 28 (1983) 6575; Phys. Rev. B 32 (1985) 158; Phys. Rev. B 30 (1984) 6774.

[13] C. Paige, J. Inst. Math. Appl. 10 (1978) 373.

VOLUME 152 (1988) Nos. 1&2
AUGUST II 1988

ISSN 0921-4526

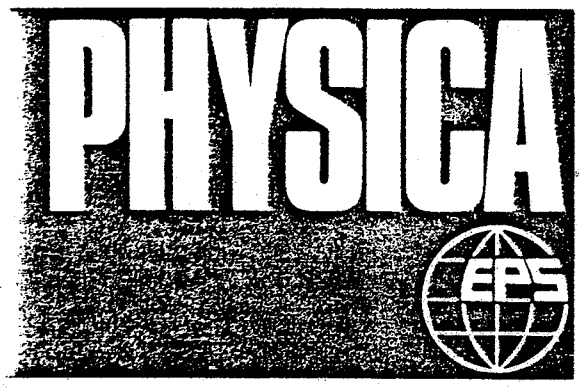

B
CONDENSED MATTER

Coherence in Superconducting Networks

Proceedings of the NATO Advanced Research Workshop on
Coherence in Superconducting Networks
Delft, The Netherlands, 14–17 December 1987

Editors:

J. E. Mooij
G. B. J. Schön

PHYBE3 152 (1&2) 1–302 (1988)

NORTH-HOLLAND AMSTERDAM